Multifunctional Structural Supercapacitor Based on Urea-Activated Graphene Nanoflakes Directly Grown on Carbon Fiber Electrodes

ACS APPLIED ENERGY MATERIALS

www.acsaem.org Article

Multifunctional Structural Supercapacitor Based on Urea-Activated Graphene Nanoflakes Directly Grown on Carbon Fiber Electrodes

Abhijit Ganguly, Anastasios Karakassides, John Benson, Shahzad Hussain, and Pagona Papakonstantinou*

Cite This: https://dx.doi.org/10.1021/acsaem.9b02469 Read Online

ACCESS | Metrics & More | Article Recommendations | Supporting Information

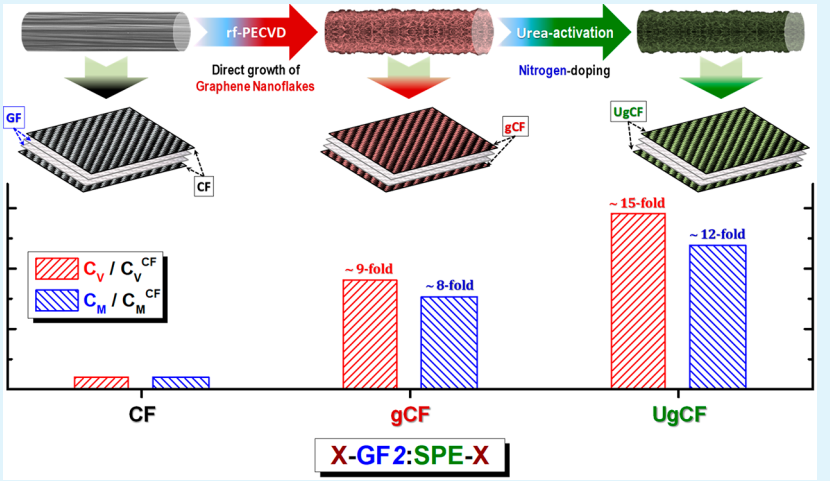

ABSTRACT: Structural energy storage systems offer both load bearing and electrochemical energy storage capabilities in a single multifunctional platform. They are emerging technologies for modern air and ground transportation vehicles, promising considerable mass and volume savings over traditional systems. To this end, carbon fiber reinforced composites have attracted interest for structural supercapacitors (SS), emanating principally from their similar laminate design. However, carbon fiber (CF) electrodes suffer from poor electrochemical storage performance. To tackle this deficiency, carbon fiber electrodes were modified with a 3D network of radially grown graphene nanoflakes (GNFs) to enhance their degree of graphitization and active surface area. We show that the GNF surface morphology offers an ~9 times increase in specific capacitance (C_{sp}) of CF structural supercapacitor. Moreover, chemical activation of the GNFs/CF hybrid electrodes by urea induces a further improvement in C_{sp} by ~14 times, while almost maintaining the elastic modulus of the control CF-based device. It has been established that the high specific capacitance stems from the highly electroactive edge-dominated nitrogen moieties and enhanced electrical conductivity induced by urea activation. Overall, the urea-activated hybrid electrodes offer an ~12-fold increase in energy and power densities compared to CF control structural supercapacitor devices. These findings provide important knowledge for the design of next-generation multifunctional energy storage electrodes by highlighting the importance of interfacial nanoengineering.

KEYWORDS: *carbon fiber reinforced polymer (CFRP) composites, solid polymer electrolyte (SPE), multifunctional structural supercapacitor (MSS), vertical graphene nanoflakes (GNFs), mechanical testing, urea activation via incipient wetness impregnation approach, nitrogen doping via urea activation*

INTRODUCTION

Structural energy storage systems are multifunctional systems which provide mechanical load bearing and electrochemical energy storage functionalities simultaneously. They have attracted great interest for electrification of aerial and ground transportation vehicles due to recent demands for weight reductions, needed to meet the CO_2 ambitious emission targets by year 2030.[1,2] Furthermore, since weight strongly influences the aircraft's power consumption, incorporation of structural energy storage systems can increase the flight endurance in small unmanned aerial vehicles (UAVs).[3]

Received: December 19, 2019
Accepted: March 5, 2020
Published: March 5, 2020

Common structural energy storage systems are in the form of batteries or supercapacitors. In contrast to conventional batteries and supercapacitors that can only store electrical energy and require external packaging to provide mechanical integrity, in structural energy systems the electrodes, separator, and electrolyte themselves are designed to impart both electrochemical energy storage and mechanical integrity, and in doing so they achieve system-level weight and volume reductions.[4−6]

Traditional carbon fiber reinforced polymer (CFRP) structural composites consist of parallel layers of high stiffness and high-strength fibers encapsulated in a polymer matrix. Conventional batteries and supercapacitors consist of ion conductive electrolytes sandwiched between parallel layers of electrically conductive electrodes. Owing to the inherent electrical conductivity of carbon fibers (CF) and the laminate structure of CFRPs, it is envisaged that CFRPs could act as multifunctional structural energy materials if appropriately engineered. Recent studies in structural supercapacitor and lithium-ion batteries show electrochemical and mechanical performance are competing properties, and a trade-off has to be made.[4−6]

The concept of structural supercapacitors was initiated by the study of Luo and Chung[7] based on a thin device made from unidirectional CF prepreg layers separated by paper dielectrics. The multifunctional performance of such device was defined and evaluated by O'Brien et al.[8] and Carlson et al.,[9] who proposed a multifunctional efficiency, η_{mf}, metric as the sum of structural (η_s) and electrical (η_e) efficiencies. This metric should exceed unity for mass-saving multifunctional design.[8−11]

The current development[12−14] of multifunctional structural supercapacitors (MSS) is mainly based on the assembly of two electrodes made of carbon fiber (CF) weave separated by a dielectric glass fiber (GF) weave separator, all bonded together with a multifunctional solid polymer electrolyte (SPE) matrix. The GF separator possesses an electrically insulating nature but sufficient accessibility to ionic transport and at the same time contributes to delamination resistance and impact strength of the structural supercapacitor.[4,5,10,13,15−18] The SPE matrix is mainly based on highly structural polymers blended with ionic liquids (ILs) or ionic salts (lithium salts, etc.) to impart the essential ionic conductivity.[10,13,15−18]

Nevertheless, the current performance of MSS is still at embryonic state, with the commercial CF being unable to deliver the expected electrochemical performances because of a lack of proper graphitization, chemical inertness, and limited active-surface area.[4−6] Because the energy storing/delivering capacity is defined by the extent of charges accumulating at the interface between the CF electrode and SPE matrix, the surface activation of CF electrodes is expected to improve the charge/discharge performance. However, it is also crucial not to compromise the mechanical properties of CF to retain the multifunctional performance.[8−10,13] Among several chemical activation processes reported so far,[13,19,20] the incipient wetness impregnation of CF with potassium hydroxide (KOH) has been claimed to offer satisfactory electrochemical enhancement without compromising the mechanical properties,[13,16,19,21,22] promoting a 5-fold improvement in specific capacitance (C_{sp}), as reported by Shirshova et al.[13]

Alternatively, providing a secondary reinforcement interface that extends into the SPE matrix, for example by covering the CF surface with carbon aerogels (CAG),[16,21,23] metal oxide (CuO, etc.) nanostructures,[18,24] or carbon nanotubes (CNTs),[10,16] was found to offer considerable improvement in the electrical or electrochemical properties of MSS, without any obvious degradation on the mechanical properties. In particular, the integration of a porous bicontinuous monolithic CAG coating has proven the most successful approach,[4,5,15,16,23] providing a 7 and 100-fold increase for MSS with GF and polypropylene separators, respectively,[15] in C_{sp} along with a raise in shear modulus (G_{12}) by 3 times (for MSS with GF separator[15]).

Graphene nanoflakes (GNFs) are three-dimensional (3D) networks of vertically oriented multiple graphene layers, also met with names of graphene nanopetals and carbon or graphene nanowalls. Recently, GNFs directly grown on carbon fibers (denoted here as *gCF*), by a catalyst-free radio frequency plasma-enhanced chemical vapor deposition (rf-PECVD),[25−27] have been demonstrated as a novel interface for improving the interfacial shear strength (IFSS) between the carbon fiber and the epoxy, with a maximum increase in IFSS of ∼118.7% without degrading the tensile strength of the underneath CF.[27] Most lately, we demonstrated that radially aligned graphene nanoflakes (GNFs),[28] grown by microwave PECVD within a few minutes, not only improve the interfacial shear strength (IFSS) by 101.5% but also lead to a remarkable 28% enhancement in the tensile strength of the hybrid fibers as observed via single-fiber tensile strength tests. Such enormous enhancement in tensile strength was associated with a reduced thermal loading on the CF due to quick GNF growth along with the elimination of harmful chemical procedures as no catalyst was required. Additionally, GNFs provided further benefits such as increased electrical conductivity (60.5% improvement for yarns and 16% for single fiber) and electrochemical capacitance (157% for yarns) in conventional electrolytes.[28] So far, GNFs have been studied as electrodes for many electrochemically based applications[29] including that of conventional supercapacitors;[30] however, their use as electrodes for structural energy storage by direct growth on CFs is an unexplored terrain.

It is anticipated that the self-assembled growth of GNFs on CF fabrics would offer the following advantages for MSS: (i) the rigid network of GNFs protrudes into the SPE matrix and hence could increase load transfer between the fiber and matrix offering increased IFSS; (ii) the porous 3D topography is enhancing the active surface area, which would be highly beneficial for enhanced charge accumulation at the *gCF*/SPE interface, resulting in enhanced capacitance; and (iii) the GNFs offer a high degree of graphitization, favoring enhanced electron-transfer efficiency, contributing to increased specific capacitance and cyclic stability.

In this paper, the focus of our study was to demonstrate the potential of urea activated GNF-coated CF (*UgCF*) for structural supercapacitors. Urea was employed as a precursor[31,32] for the nitrogen doping of *gCF* electrodes allowing transformation of the electrode to an n-type semiconductor,[30,33] providing enhanced conductivity and electrochemically active sites. The urea-activated electrode offered around 12 times higher energy and power densities compared to control CF specimens, while almost no deterioration on the elastic modulus performance demonstrating the potential of the approach for improving the multifunctionality of the CFRP-based structural supercapacitors.

https://dx.doi.org/10.1021/acsaem.9b02469
ACS Appl. Energy Mater. XXXX, XXX, XXX−XXX

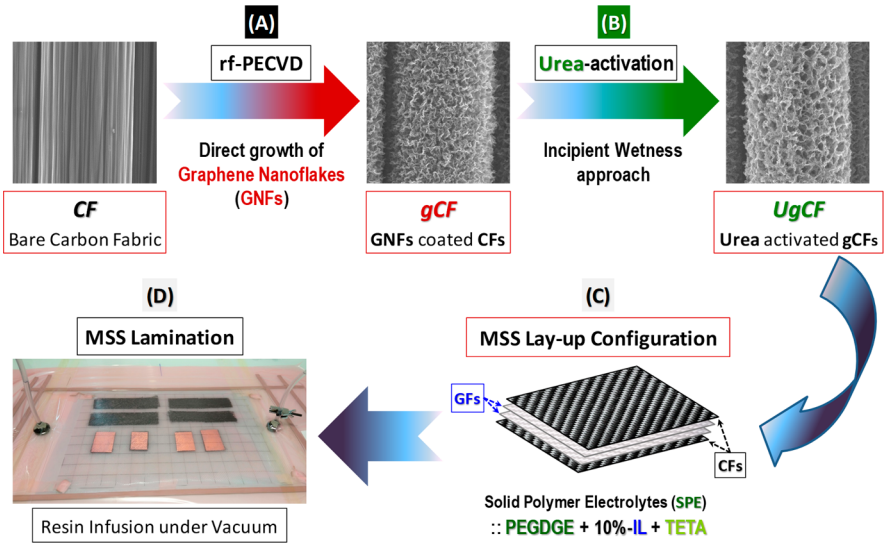

Figure 1. Schematic illustration of steps used for the fabrication of structural supercapacitor: (A) *CF* → *gCF*: direct growth of graphene nanoflakes (GNFs) on bare carbon fiber (*CF*) fabrics by rf-PECVD. (B) *gCF* → *UgCF*: urea activation of GNFs-coated carbon fiber (*gCF*) fabrics (*UgCF*). (C) CF−(2GFs:SPE)−CF lay-up configuration of multifunctional structural supercapacitor (MSS). (D) Fabrication of carbon fiber reinforced polymer (CFRP) composite-based MSS laminates via the resin infusion method.

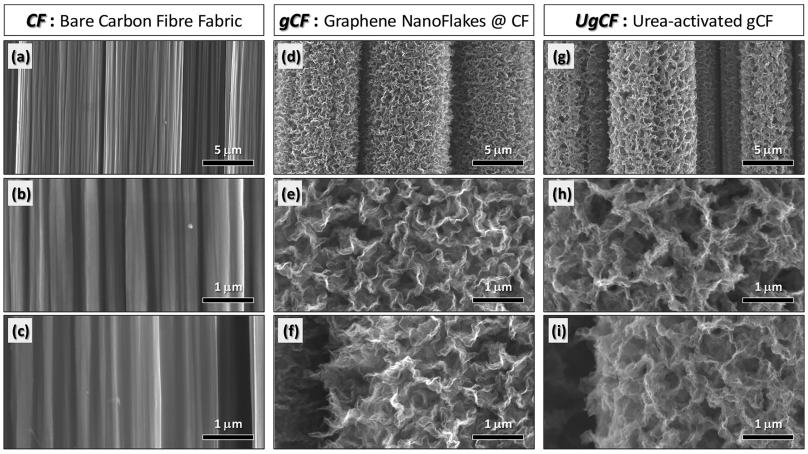

Figure 2. SEM images of different fabrics: (a−c) bare carbon fiber (*CF*); (d−f) graphene nanoflakes (GNFs) deposited at carbon fiber (*gCF*); and (g−i) Urea-activated *gCF* (*UgCF*). The second row (b, e, and h) represents images of the top surface of a single fiber, while the corresponding images of the third row (c, f, and i) illustrate the sidewall of a single fiber.

RESULTS AND DISCUSSION

A schematic representation of the steps involved in the fabrication of the structural supercapacitor is shown in Figure 1. It involves the growth of GNFs directly on bare CF (*gCF*) (Figure 1A) to enhance the degree of graphitization and increase the active surface area of CF by introducing a highly dense 3D nanoflake network of edge-oriented high-quality graphene layers. The GNFs were grown on 22 × 6 cm^2 CF woven fabrics via a radio frequency plasma-enhanced chemical vapor deposition (rf-PECVD) by using a commercial quartz tube furnace. To further improve the performance of *gCF* electrodes, a chemical activation via the incipient wetness impregnation approach (Figure 1B) was conducted by using urea.

The lay-up configuration (Figure 1C) of the structural supercapacitor involved two glass fabrics (GFs) sandwiched between two CFs fabrics (CF−(2GFs:SPE)−CF), which were infiltrated with SPE using a resin infusion process under vacuum (Figure 1D). The solid polymer electrolyte (SPE) was composed of a poly(ethylene glycol) diglycidyl ether (PEGDGE) polymeric resin, cross-linked with triethylene-tetramine (TETA) as hardener, and contained 10 wt % 1-ethyl-3-methylimidazolium bis(trifluoromethylsulfonyl)imide (EMITFSI) as ionic liquid (IL).[15−17,22]

The effects of the GNF growth and subsequent urea activation were evaluated by elemental and morphological characterizations. The improved electrochemical performances of the structural supercapacitor devices were evaluated through cyclic voltammetry (CV) and chronoamperometry (CA) employing a typical two-electrode (2E) configuration, whereas the structural performances were characterized in terms of tensile strength and elastic modulus according to the ASTM D3039 standard.[34]

Graphene Nanoflakes Directly Grown on Carbon Fiber Fabrics (*gCF*). Morphological observations revealed that *gCF* fabrics exhibit a dense and uniform coverage of GNFs (Figures 2d−f) when compared to bare *CF* fabrics (Figures 2a−c). The bright field image of a single fiber revealed a quasi-

https://dx.doi.org/10.1021/acsaem.9b02469
ACS Appl. Energy Mater. XXXX, XXX, XXX−XXX

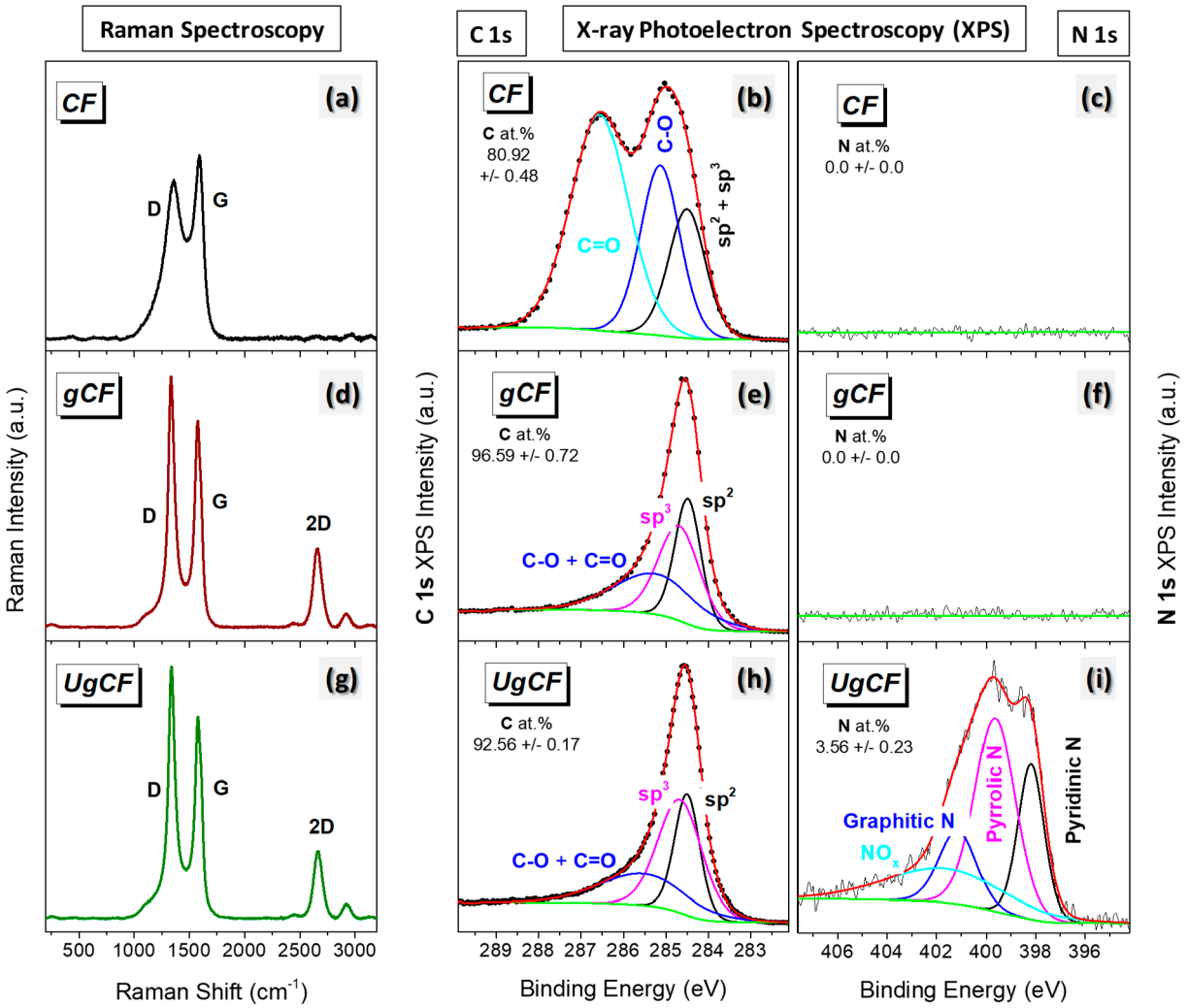

Figure 3. Raman and high-resolution X-ray photoelectron spectroscopic results. Top row: Raman (a) and high-resolution C 1s (b) and N 1s (c) XPS spectra of bare carbon fiber (*CF*) fabrics. Middle row: (d) Raman, (e) C 1s, and (f) N 1s spectra of graphene nanoflakes (GNFs) deposited on CF (*gCF*) fabrics. Bottom row: (g) Raman, (h) C 1s, and (i) N 1s spectra of urea-activated *gCF* (*UgCF*) fabrics.

maze-like network of nanoflakes, with corrugated morphology, interlaced with each other, covering the fiber surface (Figure 2e). The image of the fiber sidewall illustrated that GNFs are grown in a radial fashion, projecting vertically to the CF fiber axis (Figure 2f). Statistical analysis revealed a typical GNF loading of around 8.48 ± 0.61 wt %, as determined from the mass increment of the *gCF* fabrics relative to the bare *CF* fabrics (eq S1).

Interestingly, such preferable vertical growth of GNFs on the CF surface would undoubtedly provide a rigid 3D network of highly graphitized nanoflakes protruding into the SPE matrix, enhancing the active surface area of CF/SPE. According to the most popular growth mechanism,[35−38] the creation of self-organized vertical GNFs entails the formation of a buffer nanographitic layer parallel to the CF surface at the initial stages of growth. Under the energetic plasma conditions the hydrocarbon precursor (CH_4) is dissociated into are reactive carbon intermediates (e.g., reactive radicals and ions), which bombard the CF surface, leading to the formation of the buffer layer. The continued growth of the graphitic domains builds up stress (due to thermal and lattice mismatches), and the growing edges curl upward releasing the stress. This stage marks the onset of change in the growth direction from parallel to perpendicular. Subsequently, GNFs continue to grow in the vertical direction by (i) the attachment of the high number of radical carbon species at the active edges and/or (ii) the rapid diffusion of radical species in the direction parallel to the electric field in the sheath region of the plasma.

Both Raman and high-resolution XPS spectroscopic studies (Figure 3) clearly indicate a significant enhancement of CF graphitization following the deposition of GNFs. The *gCF* fabrics show the appearance of a characteristic 2D Raman peak of graphene (Figure 3d), along with the D and G peaks, the common vibrational features of graphitized carbon, also observed on the bare *CF* (Figure 3a). The appearance of the sharp D peak and its significant dominance over the G peak could be treated as a signature of the edge-exposed vertically aligned graphene (VG) growth.[28,35,39−41] Generally, such pronounced dominance of the D over G peak indicates the presence of disorder, arising from defects such as vacancies and edges states as well as smaller crystalline grains and ion-induced defects from the plasma-enhanced growth mechanism.[35,39−41] The VG growth originates from a stress-release mechanism of the coalescing nanographene (NG) islands, formed at the nucleation stage. Hence, the Raman signal,

https://dx.doi.org/10.1021/acsaem.9b02469
ACS Appl. Energy Mater. XXXX, XXX, XXX−XXX

recorded perpendicularly to the substrate, is dominated by the vertically exposed graphene layers and hence edge defects.[41]

The *gCF* fabrics exhibited a single C 1s peak (Figure 3e), with a high dominance of sp^2 aromatic carbon species,[42] replacing the doublet C 1s feature of *CF* associated with the presence of sizing (Figure 3b). Consequently, an increase in C:O atomic ratio from 80.9:19.1 for *CF* to 96.6:3.4 for *gCF* was found along with a rise in the total contribution of sp^2-C and sp^3-C components from 20.0 to 68.4 at. % for *CF* and *gCF*, respectively (Tables S1 and S2 present details of numerical analysis data in the Supporting Information).

It was found that the SPE loading was increased from 48.40 ± 1.53 wt % for laminates employing bare *CF* to 51.37 ± 2.34 wt % for laminates employing *gCF* electrodes. Even though the increment is low, it was observed consistently from four sets of laminates. This increase is an indication of successful impregnation of SPE in the porous GNF network.

It is evident from both cyclic voltammetry, CV (Figure 4a), and chronoamperometric, CA (Figure 4b), measurements conducted in a two-electrode (2E) configuration that the direct growth of GNFs could significantly improve the capacitive performance of MSS. Notably, the CV plots display almost linear tilted loops, indicating a high resistive behavior due to the high resistance of the solid electrolyte and high leakage current.[13,43] The slope of the loops increases with increasing the potential scan rate, as observed from Figure S1a–c. At fast scan rates the diffusion of electrolyte ions into the electrode's internal structure (pores) become more difficult (diffusion limitation),[18,43,44] leading to insufficient DLC distribution at the SPE/CF interface and hence to a decrease of the specific capacitance (C_{sp}) values (Figure S1d,e). In simple words, the MSS will not be capable of holding its voltage after being charged during CV, even at 10 mV/s. That is why, in this study, a transient charge–discharge (CA) method[13,43] was utilized to measure capacitance, similarly to a previous study by Shirshova et al.[13]

The C_{sp} values (Figure 4c) were determined via fitting the charge–discharge responses to the RC equivalent circuit model (inset Figure 4b) via eqs S2–S4. GNFs allowed significant improvements in C_V (50.99 mF/cm^3) and C_M (30.82 mF/g) values of *gCF*-MSS (Figure 4d). In comparison, typical *CF*-MSS exhibited C_V and C_M values of only 5.65 mF/cm^3 and 4.02 mF/g, respectively, which are in agreement with earlier reports on a similar PEGDGE (with 10 wt % IL) matrix based CFRP-MSS with GF separator.[13,15,22]

Unfortunately, the measured absolute values of C_{sp} are difficult to be compared with other values reported in the literature. A literature survey shows a range of different characterization methods and different approaches for C_{sp} estimation; this along with variations in the quality of commercial CF fabrics employed, types and numbers of the separators used, and types and compositions of the SPE matrices involved make meaningful comparisons even more difficult.

A comparison of the performance of CFRP-MSS studied here with the reported literature (Table S5) shows comparable C_{sp} values with the earlier studies on similar PEGDGE-polymer-based MSS.[13,15,16] Although the CAG-coated CF electrodes showed higher C_M values of around 90.5 mF/g,[16] compared to the *gCF*-MSS (30.82 mF/g), the better performance in these earlier studies[15,16] is related to the use of single GF separator for their capacitance measurements and double GF separators for their mechanical measurements

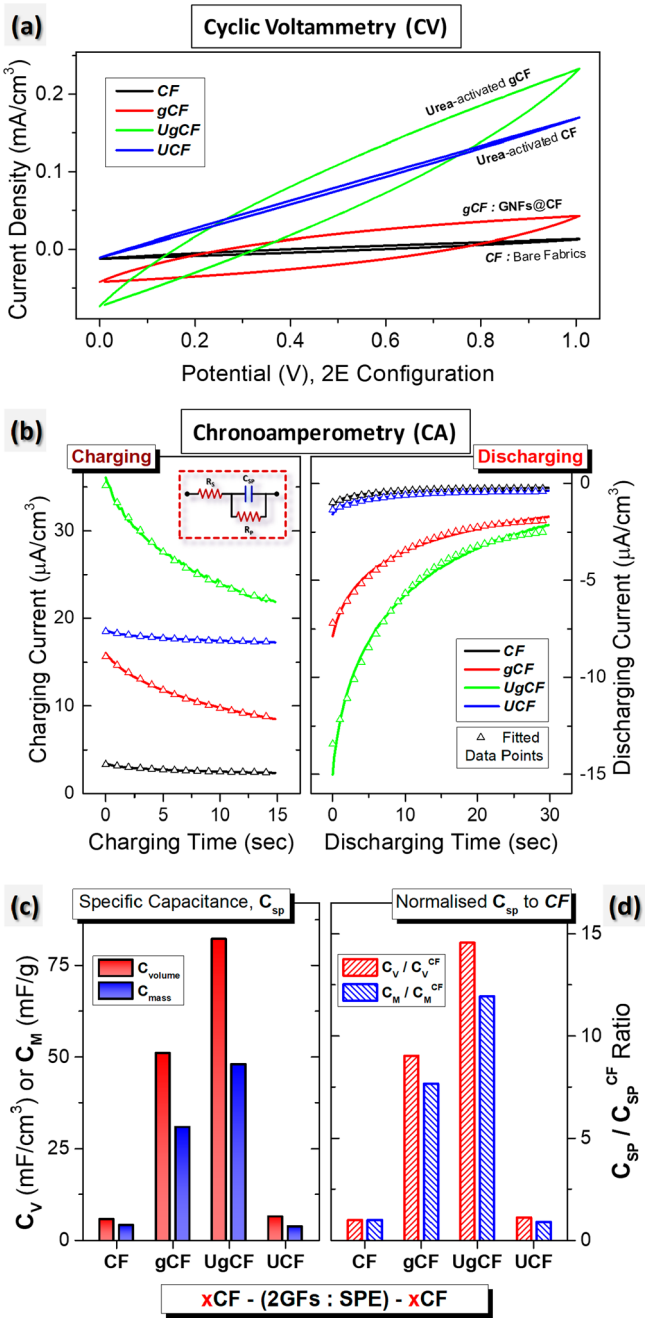

Figure 4. (a) Cyclic voltammetry (CV) plots, recorded in a two-electrode (2E) configuration, at a scan rate of 10 mV/s, for the MSS devices based on bare carbon fiber (*CF*) fabric, graphene nanoflakes (GNFs) deposited on CF (*gCF*), urea-activated *gCF* (*UgCF*), and urea-activated carbon fiber (*UCF*). (b) Respective chronoamperometric (CA) curves, recorded in 2E configuration, applying 0.1 V step potential, representing the charge (left) and discharge (right) performances. The fitted data points were calculated by fitting the CA charge and discharge data, using eqs S2 and S3, respectively, to the current transient response of the RC equivalent circuit model[13,15,16] (simplified Randles cell, inset of part b). (c) Specific capacitance (C_{sp}) derived from eq S4. (d) Normalized specific capacitance values (C_{sp}/C_{sp}^{CF}) values.

(Table S5). In our study, for consistency purposes, we utilized the CF–(2GFs:SPE)–CF lay-up configuration, which involved two layers of GF separators, for both electrochemical and mechanical characterization. On the other hand, Javaid et

https://dx.doi.org/10.1021/acsaem.9b02469
ACS Appl. Energy Mater. XXXX, XXX, XXX–XXX

al.[17,19,22,23] have employed a single separator for PEGDGE-polymer-based MSS utilizing the CA method for C_{sp} calculation, but with longer charging time (1500 s), without employing the "fitting" approach suggested by Shirshova et al.[13] Their methodology resulted[22] in C_V values of around 90 mF/cm^3 for PEGDGE-polymer MSS based on KOH-activated CFs, much higher compared to *gCF*-MSS (50.99 mF/cm^3). Through a completely different approach, Deka et al.[5,18,24] have utilized galvanostatic charge−discharge (GCD) measurements, similar to those used for characterizing conventional solution-based supercapacitors,[45−47] and achieved an extremely high C_M value of around 28.63 F/g (for CuCoSe nanowires-coated CF-based MSS).[24] However, to perform the GCD measurements, Deka et al.[5,18,24] immersed/soaked the MSS device in highly concentrated (3 M) KCl aqueous electrolyte, enhancing the accessibility of elecrolyte ions into the internal structure of CF electrodes, which was responsible for facilitating efficient charge−discharge at the CF/SPE interfaces.

Here, we propose the normalized ratio of specific capacitance (C_{sp}/C_{sp}^{CF}) to represent the improvement on C_{sp} of a MSS, over that of bare CF-MSS (C_{sp}^{CF}). Compared to other values reported in the literature[13,15,16,22−24] (Table S5), the normalized (C_{sp}^{gCF}/C_{sp}^{CF}) values of *gCF*-MSS presented in Figure 4d (and Table S3) clearly evidence a distinctive improvement in specific capacitance, induced by the GNF morphology.

Such improvement is attributed to the reduced R_S (4.51 kΩ·cm^2) and R_P (2.4 kΩ·cm^2) but enhanced τ (8.58 s) values for *gCF*-MSS (see the Supporting Information, eqs S2−S4, for definitions of R_S, R_P, and τ parameters). The respective R_S, R_P, and τ values for *CF*-MSS were found to be 31.6 kΩ·cm^2, 11.4 kΩ·cm^2, and 5.55 s, respectively. The series resistance R_S depends on a number of factors including the active area, porosity, and electrical resistance of the electrodes as well as the ionic resistance of the electrolyte and interfacial resistance between the electrolyte and electrode.[13,15] Hence, the drop in R_S for *gCF*-MSS may indicate an improvement in electrical conductivity of *gCF* electrode and/or reduction of resistance at the *gCF*/SPE interface. However, the use of copper tape as a current collector limits any substantial reduction in R_S. Here, it is worth mentioning that such an extremely high R_S value is the main reason for the failure of the CV method as an C_{sp} measurement tool, as discussed earlier. Such a claim is further justified by the lower measured values of C_{sp} obtained from CV studies (Figure S1d), relative to those measured by fitting the CA data (Figure 4c).

The simultaneous reduction in R_P (resistance in parallel) and increase in τ (discharging time constant) values observed in *gCF*-MSS also indicate enhanced capacitive properties as supported by eq S4. Overall, the GNF interface improves the C_{sp} by 8−9 times (C_{sp}^{gCF}/C_{sp}^{CF}) compared to its bare counterpart. The estimated energy density (Γ_M) increased from 5.59 to 42.81 μWh/kg, while the power density (P) increased from 63.27 to 456.17 mW/kg, yielding ∼7.7 and 7.2 times improvements in energy and power densities, respectively (Table S3).

The advantages of GNFs were also evident via a comparative study of *gCF* electrodes with different GNFs loadings (Figure S2). Higher loading led to an enhancement of C_{sp} values (Figure S3).

Effect of Urea Activation of Carbon Fiber Fabrics. Although *gCF* electrodes improved the capacitive performance of MSS, further improvement was sought by employing surface activation of the *gCF*. Such activation was performed by incipient wetness impregnation of *gCF* and bare *CF* electrodes in highly concentrated urea solution followed by heat treatment.

Here, urea was intentionally employed as a precursor for nitrogen doping,[31,32] with a view of improving the electrical conductivity of the *gCF* electrodes, since it is well-known that nitrogenation of graphene leads to improved electron transfer. This hypothesis was confirmed by the appearance of N 1s XPS signal on urea-activated *gCF* fabrics (*UgCF*) displaying a C:N:O atomic ratio of 92.56:3.56:3.88 (Figure 3i and Table S1). No degradation in morphology could be observed from the SEM analysis (Figure 2g−i), except for a minute folding effect at the open ends of nanoflakes—an effect resulting from the soaking process in aqueous solution. Hence, it can be considered that the chemical activation of *gCF* fabrics with urea does not lead to any degradation in GNFs morphology or its graphitic nature, but it induces N-doping (3.88 at. %) on the *UgCF* fabrics.

The retention of the graphitic nature was also evidenced from the sp^2-dominated C 1s XPS signal (Figure 3h, with the total contribution of sp^2 and sp^3 C species around 74.4 at. % (Table S2) and the graphene-specific 2D Raman signal (Figure 3g). A slight reduction of I_G/I_D values (Table S1), from *gCF* (0.71) to *UgCF* (0.68), can be observed that is principally attributed to the substitutional N-doping phenomena (Table S2). As evidenced by the high-resolution N 1s XPS (Figure 3i and Figure S6e), N atoms were doped by substituting C atoms either at the edge (pyridinic-N and pyrrolic-N) or on the basal planes (graphitic-N) of the graphene (Table S2).[30,33] Such substitutional doping with group V element (N atom) in group IV element (C structure) would lead to an enhanced conductivity as well as improved capacitance,[30−33] which is evidenced from the electrochemical characterizations (Figures 4a,b).

As expected, the nitrogen-doped urea-activated *UgCF* electrodes improved the capacitive performance of CF-based MSS laminates, resulting in the highest observed C_V of 82.25 mF/cm^3 and C_M of 47.98 mF/g (Figure 4c) values, yielding 14.57 (C_V^{UgCF}/C_V^{CF}) and 11.93 (C_V^{UgCF}/C_V^{CF}) times increases in the volumetric and gravimetric C_{sp} values of *CF*-MSS, respectively (Figure 4d). As in our earlier observations for *gCF*-MSS, the *UgCF*-MSS also exhibited reduced R_S (4.38 kΩ·cm^2) and R_P (1.43 kΩ·cm^2) values and an enhanced τ (8.63 s). *UgCF*-MSS displayed energy Γ_M and power densities P_M of 66.64 μWh/kg and 787.81 mW/kg, respectively. Overall, the *UgCF*-MSS offered around 11.93 times higher $\Gamma_M^{UgCF}/\Gamma_M^{CF}$ relative to the *CF*-based MSS (Table S3). Improvements on RC circuit parameters by the growth of GNFs and the subsequent urea activation were also further supported from the electrochemical impedance spectroscopy (EIS) measurements (Figure S4). Nyquist plots (Figure S4a) clearly exhibit an overall reduction on both the real (Z') and imaginary (Z'') impedance values associated with the observed reduction of R_S and R_P values for both *gCF*- and *UgCF*-MSS. Likewise, the Bode plots show a reduction in the absolute magnitude of total impedance Z (Figure S4b). These findings consistently confirm that the enhancement of CF graphitization and surface activation greatly improved the electrochemical charge/discharge performances of CF-MSS.

For comparison, the bare *CF* fabrics as also subjected to the proposed urea-activation process. The urea-activated bare CF electrodes (*UFC*) also exhibited substantial N-doping (1.38 at.

https://dx.doi.org/10.1021/acsaem.9b02469
ACS Appl. Energy Mater. XXXX, XXX, XXX−XXX

%, Figure S6) without any obvious effect on morphology as observed from the SEM images (Figure S5). Importantly, as described in the Experimental Details section, all the carbon fabrics (*CF* and *gCF*), after the urea-activation step, and all the treated fabrics (*UgCF* and *UCF*) were subjected to minimum 2−3 washes with double-distilled water, confirming the complete removal of any unreacted "urea" crystallite residues, as established by the SEM observations (Figure 2 and Figure S5). Hence, it could be confirmed that the N signal, achieved by the surface-sensitive XPS characterization, is solely originated from the urea-activated carbon fibers, and not from any crystallite residues of urea-precursors.

However, comparative XPS studies have revealed that the *UCF* fabrics (Figure S6e) possess a higher amount of graphitic N-species (N-doping at the basal plane of graphene layers) over pyridinic, while the *UgCF* fabrics owned both pyridinic and pyrrolic N-species (N-doping at the graphene edges) in addition to graphitic ones, with the pyrrolic N-species being predominant (Figure S6h and Figure 3i). The basal-N species, like graphitic-N, being positively charged have an enhancing effect on capacitance, in terms of improved electron transfer in the graphitic plane,[31,32] which is evidenced from the improved current density observed for *UCF* (Figures 4a,b) compared to its nonactivated counterpart (*CF*). On the other hand, the edge-N species, like pyridinic-N and pyrrolic-N, are the most effective functional groups in improving the energy storage performance mainly due to their pseudocapacitive contribution.[30−33] For *UgCF*, the total contribution of the edge-N species was found to be around 63.70 at. %, while it was only 19.01 at. % for *UCF* (Table S2). As a consequence, the substantial improvement observed on the capacitive performance of *UgCF*-MSS over its bare CF counterpart (Figures 4c,d) is attributed to a combination of factors originating from (i) the high surface area of graphene nanoflakes and (ii) the presence of a higher amount of N species with (iii) dominance of edge-N species over the basal-N.

The chemical activation of *gCF* was also performed by impregnating it in a mixture of urea and KOH, with different urea:KOH molar ratios. The chemical activation of conventional *CF* fabrics with KOH has been claimed to offer the significant enhancement in the surface area of CF fabrics without compromising its mechanical properties,[13,16,19,21,22] improving its performances as an electrode for MSS applications. However, in our study, KOH activation of *gCF* electrode (*U0g*, urea:KOH = 0:1) induced an alarming loss of GNFs (Figures S7d−f) confirmed by both SEM and Raman observations, where spectra similar to those of bare *CF* were recorded at many probed areas. Furthermore, XPS studies showed a significant reduction of the C:O atomic ratio from 96.59:3.41 (*gCF*, Figure S8a−c) to 24.29:75.71 (*U0g*, Figure S8d,e) for KOH activated fibers. As expected, *U0g*-MSS exhibited reduced C_{sp} values (Figure S9a) and a corresponding normalized C_M^{U0g}/C_M^{gCF} value much lower than unity (Figure S9b), relative to the *gCF*-MSS (C_{sp}^{gCF}). As the urea content increased in the urea:KOH mixture, the retention of the grown GNFs structures on the CF fabrics was evidenced from the SEM studies (Figures S7g−o), accompanied by an improvement of C:O atomic ratio and the appearance of nitrogen signals (Figure S8g−o). The capacitive performance of urea:KOH activated-*gCF*- MSS was improved significantly (Figure S9a), with a monotonous rise in the normalized C_{sp}/C_{sp}^{gCF} values (Figure S9b) as the urea content was increased in the activation mixture solution. Nevertheless, the best performance was achieved from the pure urea-activated *gCF* electrode (*U4g*, urea:KOH = 1:0), with C_M^{UgCF}/C_M^{gCF} around 1.5.

We should note that the term "activation" is commonly used for the conventional chemical treatment of CF fabrics with KOH like etchants, which has been claimed to offer an enhancement in the "active surface area" of CF fabrics by introducing porosity and oxygen functional groups. Here, it would be important to mention that the proposed "urea-activation" term denotes the activation of *CF* or *gCF* electrodes by improving their electrical conductivity via an intentional N-doping without altering their porosity. The reaction mechanism of carbon fiber with urea does not include removal of carbon atoms and hence does not produce any etching or porous morphology. This is also established by the SEM images of Figure 5S, where no significant difference was between bare and urea-treated CFs.

Overall, the *UgCF* reinforced polymer-based MSS shows considerable improvement over the bare CFRP control device (Table S3). As compared with the literature data (Table S5), the proposed development of the CF electrode can be a promising approach for the future MSS applications.

Similarly to other reported structural supercapacitors, even though *UgCF*- or *gCF*-MSS exhibits lower C_{sp} values relative to the conventional solution-based supercapacitors,[4] they demonstrated outstanding stability showing no significant degradation (Figure S10). Both the bare and modified CF electrodes exhibited very stable cycle life spanning from 97% to 101% over 5000 CA cycles (Figure S10d,e), a behavior linked to the structure of the solid electrolyte.

Mechanical Properties and Multifunctionality of *gCF*- and *UgCF*-Based MSS. For an MSS device, it is essential that the mechanical performance of CFRC is not severely comprised at the expense of electrochemical performance, and vice versa. Notably, the capacitive performance of an MSS device cannot be better than that of a conventional "monofunctional" supercapacitor mainly because of the high ionic resistance of the structural SPE matrix. Similarly, its mechanical performance cannot beat a "monofunctional" structural laminate because of the presence of a multifunctional SPE and the presence of interleave (separator) between the CF layers. However, a balance between the conflicting electrochemical and mechanical properties should be achieved to maintain the mass-saving design of a "multifunctional" system.[8−11]

All three, *CF* and modified *gCF* and *UgCF* MSS, exhibited a linear stress vs strain behavior (Figure S11a) for the in-plane tensile test until failure.[11,18,34,48] The mechanism for this failure is delamination either between separator and matrix or between carbon fibers and separator, and it is common for all CFRP laminates interleaved with a less stiff separator,[11,48] in an ionic SPE matrix. As observed from Figure S11, both *gCF*- and *UgCF*-MSS exhibited mechanical performances inferior to bare *CF*-MSS, due to delamination between CF electrodes and GF separators, and have been triggered at an earlier stage compared to bare *CF*-MSS.

Because all three devices are composed of the same GF separator and PEGDGE-based epoxy, the resulting degradation of tensile strength (σ) values on *gCF* and *UgCF* -MSS (Figure 5a) may have resulted from an increased thermal loading on the CFs during the processes used to produce the GNFs and activated GNFs. It should be mentioned that the manual handling of the CF fabrics during every processing step resulted in loss of carbon fibers from the outer edges, which

https://dx.doi.org/10.1021/acsaem.9b02469
ACS Appl. Energy Mater. XXXX, XXX, XXX−XXX

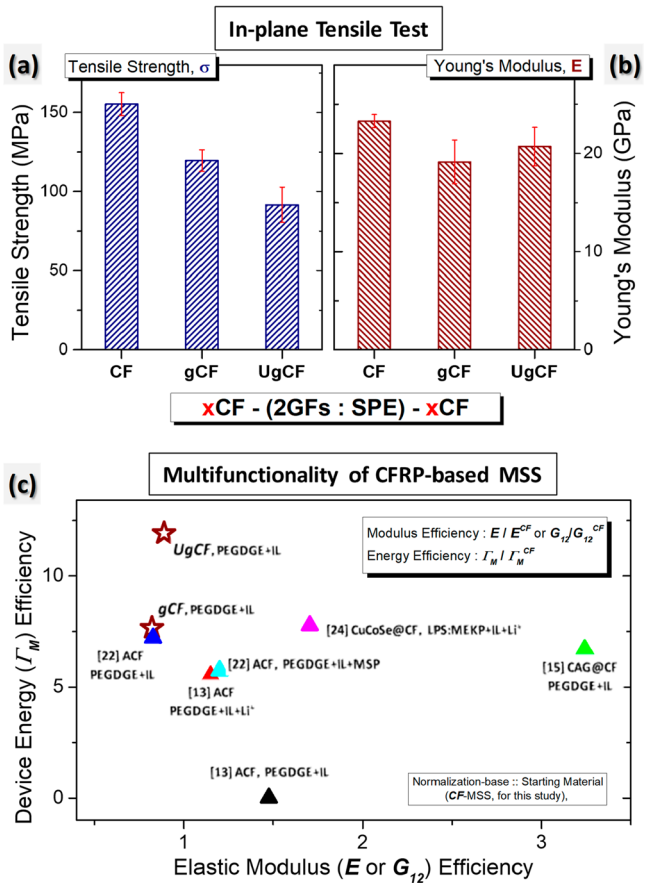

Figure 5. Comparison of (a) tensile strength (σ) and (b) Young's modulus (E) values of various CFRP laminates, consisting of bare carbon fiber (*CF*), graphene nanoflakes (GNFs) deposited on CF (*gCF*), and urea-activated *gCF* (*UgCF*), with CF−(2GFs:SPE)−CF lay-up configuration incorporating two layers of glass fiber (GF) fabric separators. (c) Multifunctional performance, device energy efficiency (normalized energy density, Γ_M/Γ_M^{CF}) vs elastic modulus efficiency (normalized Young's modulus, E/E^{CF} (for current study and refs 13 and 24) or shear modulus, G_{12}/G_{12}^{CF} (for refs 15 and 22)) of *gCF*- and *UgCF*-based MSS, in comparison to other published MSS systems. The reference numbers have been indicated along with the modified CF electrodes and SPE matrices. For every modified CF electrode, its unmodified counterpart (*CF*-MSS, for our case) has been treated as the "base device" for the normalization. ACF = KOH-activated CF, CAG@CF = carbon aerogel-coated CF, CuCoSe@CF = copper cobalt selenide nanowires grown on CF, PEGDGE = poly(ethylene glycol) diglycidyl ether, IL = ionic liquid, Li^+ = lithium ionic salt, MSP = mesoporous silica particles, LPS = unsaturated polyester resin, and MEKP = methyl ethyl ketone peroxide.

also led to a reduced packing density of the woven fabrics. The elastic moduli (Young's modulus, E) of *gCF* (19.13 ± 2.24 GPa) and *UgCF* (20.72 ± 1.97 GPa) based MSS were also found to decrease with respect to *CF*-MSS (23.30 ± 0.65 GPa) (Figure 5b), but to a much lower degree compared to tensile strength. The normalized elastic moduli (E/E^{CF}) were found to be 0.82 and 0.89 for *gCF* and *UgCF* -MSS, respectively (Table S4).

Figure 5c represents the "multifunctional" performance of the proposed MSS devices, correlating the device energy efficiency (Γ_M/Γ_M^{CF}) against the mechanical elastic modulus efficiency (E/E^{CF}). A comparison with the other published works on MSS systems[13,15,22,24] reveals that the proposed modification of commercial CF electrodes, even though is not showing promising structural performance, could substantially outperform other MSS in terms of their electrochemical capacitive storage. Especially, the urea-activated GNFs on CF (*UgCF*) electrodes offered around 12 times gain in energy density efficiency ((Γ_M/Γ_M^{CF}), with only a small loss (≈ 0.89) in elastic modulus efficiency (E/E^{CF}) demonstrating a novel and promising approach for improving the "multifunctionality" of the CFRP-based MSS.

CONCLUSIONS

In this work, we investigated the electrochemical and mechanical performance of a structural supercapacitor based on graphene nanoflakes (GNFs) directly grown on carbon fabric (CF) electrodes, infused in a mixture of PEGDGE polymer matrix and ionic liquid (EMITFSI) electrolyte. Direct growth of GNFs on CF by rf-PECVD method led to a significant enhancement of the specific capacitance (C_{sp}) by ∼9 times compared to control bare *CF* MSS device and a 7.5 times improvement in capacitive energy density (Γ_M). Importantly, activation of GNF-coated fabrics (*UgCF*) by a novel method in a concentrated urea solution introduced a 3.5 at. % nitrogen doping to the hybrid fabrics, which commanded 14- and 12-fold leaps in specific capacitance and energy density, respectively, relative to control MSS device consisting of bare CF electrodes. The urea activated GNF/CF hierarchical based structural supercapacitors display improvements in the electrochemical performance due to the combined effects of (i) increased graphitized surface area promoting ion accumulation, (ii) high conductivity induced by nitrogen doping, favoring electron transfer efficiency, and (iii) good electrical contact to the CF induced by the direct growth of GNFs. The urea-activated GNF-based device offered an energy efficiency of 12 and a structural efficiency of 0.9 in terms of Young's modulus, showing potential for "multifunctional" applications.

EXPERIMENTAL DETAILS

Growth of Graphene Nanoflakes on Carbon Fiber Fabrics by rf-PECVD. Graphene nanoflakes (GNFs) were grown directly on the as-purchased bare carbon fiber (*CF*) fabrics via a commercial radio frequency plasma enhanced chemical vapor deposition system (rf-PECVD; Zhengzhou Protech Technology Co. Ltd., China). The GNF deposition was performed under pure CH_4 gas flow of 10 sccm and a sustained plasma was obtained at an rf power of 500 W. The substrate temperature was maintained at around 800 °C during the 1 h deposition. The GNF-coated carbon fiber fabrics are denoted as *gCF*.

Typical GNF loading was found to be around 8.48 ± 0.61 wt % for the particular growth conditions mentioned above.

Urea Activation of Bare and GNFs-Coated Carbon Fiber Fabrics. Urea activation was performed by an incipient wetness impregnation of CF fabrics in highly concentrated urea solution followed by heat treatment. First, both bare *CF* and *gCF* fabrics were soaked in Petri dishes for 8 h in 1.85 M urea solution at room temperature. Subsequently, the impregnated CF fabrics were dried in a vacuum oven at 80 °C overnight. The urea loading was determined after drying and was found to be 12.98 ± 0.98 and 10.07 ± 0.52 wt % for *CF* and *gCF* fabrics, respectively. This was followed by heat treatment of the dried fabrics at 800 °C for 30 min under pure Ar gas (flow rate of 10 sccm). Finally, all the activated CF fabrics were washed carefully with distilled water (minimum 2−3 washes with double-distilled water) and dried in a vacuum oven at 80 °C overnight. The urea-activated bare and GNFs-coated CF fabrics are denoted as *UCF* and *UgCF*, respectively.

For a comparative study, the chemical activation of *gCF* was also performed by impregnation in a mixture of urea and KOH. Fabric

https://dx.doi.org/10.1021/acsaem.9b02469
ACS Appl. Energy Mater. XXXX, XXX, XXX−XXX

specimens impregnated in Urea:KOH molar ratios of 0:1, 1:2, 1:1, 2:1, and 1:0, are denoted as *U0g*, *U1g*, *U2g*, *U3g*, and *U4g*, respectively.

■ ASSOCIATED CONTENT

Supporting Information

The Supporting Information is available free of charge at https://pubs.acs.org/doi/10.1021/acsaem.9b02469.

Experimental details (fabrication, characterizations); equations used to calculate the measured parameters; tables for the numerical analysis of Raman and XPS spectroscopic data; figures for the supporting studies on the effect of GNFs loading, urea activation of bare CF, chemical activation with a mixture of KOH and urea, and tensile stress−strain curves (PDF)

■ AUTHOR INFORMATION

Corresponding Author

Pagona Papakonstantinou − *School of Engineering, Engineering Research Institute, Ulster University, Newtownabbey BT37 0QB, United Kingdom;* orcid.org/0000-0003-0019-3247; Email: p.papakonstantinou@ulster.ac.uk

Authors

Abhijit Ganguly − *School of Engineering, Engineering Research Institute, Ulster University, Newtownabbey BT37 0QB, United Kingdom;* orcid.org/0000-0002-8852-2721

Anastasios Karakassides − *School of Engineering, Engineering Research Institute, Ulster University, Newtownabbey BT37 0QB, United Kingdom*

John Benson − *Core Technology Facility, 2-DTech, Manchester M13 9NT, United Kingdom*

Shahzad Hussain − *School of Engineering, Engineering Research Institute, Ulster University, Newtownabbey BT37 0QB, United Kingdom*

Complete contact information is available at: https://pubs.acs.org/10.1021/acsaem.9b02469

Notes

The authors declare no competing financial interest.

■ ACKNOWLEDGMENTS

The authors acknowledge support from the Air Force Office of Scientific Research (AFOSR) under Grant FA9550-17-1-0042 and the Department of Education in Northern Ireland and Ulster University for providing a PhD studentship to A.K.

■ REFERENCES

(1) Schäfer, A. W.; Barrett, S. R. H.; Doyme, K.; Dray, L. M.; Gnadt, A. R.; Self, R.; O'Sullivan, A.; Synodinos, A. P.; Torija, A. J. Technological, Economic and Environmental Prospects of All-Electric Aircraft. *Nat. Energy* **2019**, *4*, 160−166.

(2) Making the Transition to Zero-Emission Mobility. In 2019 ACEA Progress Report, Enabling Factors for Alternatively-Powered Cars in the EU; European Automobile Manufacturers Association, 2019.

(3) Schlichting, A. D.; Eisenbeiser, K. Multifunctional Power Systems for Improved Size, Weight, and Power (Swap) in Portable Electronic Systems; 2015; page retrieved from www.mitre.org.

(4) Asp, L. E.; Greenhalgh, E. S. Structural Power Composites. *Compos. Sci. Technol.* **2014**, *101*, 41−61.

(5) Deka, B. K.; Hazarika, A.; Kim, J.; Park, Y.-B.; Park, H. W. Recent Development and Challenges of Multifunctional Structural Supercapacitors for Automotive Industries. *Int. J. Energy Res.* **2017**, *41*, 1397−1411.

(6) Chung, D. D. L. Development, Design and Applications of Structural Capacitors. *Appl. Energy* **2018**, *231*, 89−101.

(7) Luo, X.; Chung, D. D. L. Carbon-Fiber/Polymer-Matrix Composites as Capacitors. *Compos. Sci. Technol.* **2001**, *61*, 885−888.

(8) O'Brien, D. J.; Baechle, D. M.; Wetzel, E. D. Design and Performance of Multifunctional Structural Composite Capacitors. *J. Compos. Mater.* **2011**, *45*, 2797−2809.

(9) Carlson, T.; Ordéus, D.; Wysocki, M.; Asp, L. E. Structural Capacitor Materials Made from Carbon Fibre Epoxy Composites. *Compos. Sci. Technol.* **2010**, *70*, 1135−1140.

(10) Greenhalgh, E. S.; Ankersen, J.; Asp, L. E.; Bismarck, A.; Fontana, Q. P. V.; Houlle, M.; Kalinka, G.; Kucernak, A.; Mistry, M.; Nguyen, S.; Qian, H.; Shaffer, M. S. P.; Shirshova, N.; Steinke, J. H. G.; Wienrich, M. Mechanical, Electrical and Microstructural Characterisation of Multifunctional Structural Power Composites. *J. Compos. Mater.* **2015**, *49*, 1823−1834.

(11) Snyder, J. F.; Gienger, E. B.; Wetzel, E. D. Performance Metrics for Structural Composites with Electrochemical Multifunctionality. *J. Compos. Mater.* **2015**, *49*, 1835−1848.

(12) Snyder, J.; Carter, R.; Wong, E.; Nguyen, P.; Xu, K.; Ngo, E.; Wetzel, E. Multifunctional Structural Composite Batteries. *Int. SAMPE Technol. Conf.* **2007**, 18.

(13) Shirshova, N.; Qian, H.; Shaffer, M. S. P.; Steinke, J. H. G.; Greenhalgh, E. S.; Curtis, P. T.; Kucernak, A.; Bismarck, A. Structural Composite Supercapacitors. *Composites, Part A* **2013**, *46*, 96−107.

(14) Ciocanel, C.; Browder, C.; Simpson, C.; Colburn, R. The Challenges of Achieving Good Electrical and Mechanical Properties When Making Structural Supercapacitors. *Proc. SPIE* **2013**, *8689*, 17.

(15) Qian, H.; Kucernak, A. R.; Greenhalgh, E. S.; Bismarck, A.; Shaffer, M. S. P. Multifunctional Structural Supercapacitor Composites Based on Carbon Aerogel Modified High Performance Carbon Fiber Fabric. *ACS Appl. Mater. Interfaces* **2013**, *5*, 6113−6122.

(16) Shirshova, N.; Qian, H.; Houllé, M.; Steinke, J. H. G.; Kucernak, A. R. J.; Fontana, Q. P. V.; Greenhalgh, E. S.; Bismarck, A.; Shaffer, M. S. P. Multifunctional Structural Energy Storage Composite Supercapacitors. *Faraday Discuss.* **2014**, *172*, 81−103.

(17) Javaid, A.; Ho, K. K. C.; Bismarck, A.; Steinke, J. H. G.; Shaffer, M. S. P.; Greenhalgh, E. S. Carbon Fibre-Reinforced Poly(Ethylene Glycol) Diglycidylether Based Multifunctional Structural Supercapacitor Composites for Electrical Energy Storage Applications. *J. Compos. Mater.* **2016**, *50*, 2155−2163.

(18) Deka, B. K.; Hazarika, A.; Kim, J.; Park, Y.-B.; Park, H. W. Multifunctional CuO Nanowire Embodied Structural Supercapacitor Based on Woven Carbon Fiber/Ionic Liquid−Polyester Resin. *Composites, Part A* **2016**, *87*, 256−262.

(19) Javaid, A.; Ho, K. K. C.; Bismarck, A.; Shaffer, M. S. P.; Steinke, J. H. G.; Greenhalgh, E. S. Multifunctional Structural Supercapacitors for Electrical Energy Storage Applications. *J. Compos. Mater.* **2014**, *48*, 1409−1416.

(20) Li, S.; Zhao, Y.; Zhang, Z.; Tang, H. Preparation and Characterization of Epoxy/Carbon Fiber Composite Capacitors. *Polym. Compos.* **2015**, *36*, 1447−1453.

(21) Qian, H.; Diao, H.; Shirshova, N.; Greenhalgh, E. S.; Steinke, J. G. H.; Shaffer, M. S. P.; Bismarck, A. Activation of Structural Carbon Fibres for Potential Applications in Multifunctional Structural Supercapacitors. *J. Colloid Interface Sci.* **2013**, *395*, 241−248.

(22) Javaid, A.; Ho, K. K. C.; Bismarck, A.; Steinke, J. H. G.; Shaffer, M. S. P.; Greenhalgh, E. S. Improving the Multifunctional Behaviour of Structural Supercapacitors by Incorporating Chemically Activated Carbon Fibres and Mesoporous Silica Particles as Reinforcement. *J. Compos. Mater.* **2018**, *52*, 3085−3097.

(23) Javaid, A.; Irfan, M. Multifunctional Structural Supercapacitors Based on Graphene Nanoplatelets/Carbon Aerogel Composite Coated Carbon Fiber Electrodes. *Mater. Res. Express* **2019**, *6*, 016310.

(24) Deka, B. K.; Hazarika, A.; Kim, J.; Kim, N.; Jeong, H. E.; Park, Y.-B.; Park, H. W. Bimetallic Copper Cobalt Selenide Nanowire-

Anchored Woven Carbon Fiber-Based Structural Supercapacitors. *Chem. Eng. J.* **2019**, *355*, 551−559.
(25) Chi, Y.; Chu, J.; Chen, M.; Li, C.; Mao, W.; Piao, M.; Zhang, H.; Liu, B. S.; Shi, H. Directly Deposited Graphene Nanowalls on Carbon Fiber for Improving the Interface Strength in Composites. *Appl. Phys. Lett.* **2016**, *108*, 211601.
(26) Wang, X.; Li, C.; Chi, Y.; Piao, M.; Chu, J.; Zhang, H.; Li, Z.; Wei, W. Effect of Graphene Nanowall Size on the Interfacial Strength of Carbon Fiber Reinforced Composites. *Nanomaterials* **2018**, *8*, 414.
(27) Sha, Z.; Han, Z.; Wu, S.; Zhang, F.; Islam, M. S.; Brown, S. A.; Wang, C.-H. Low-Temperature Plasma Assisted Growth of Vertical Graphene for Enhancing Carbon Fibre/Epoxy Interfacial Strength. *Compos. Sci. Technol.* **2019**, *184*, 107867.
(28) Karakassides, A.; Ganguly, A.; Tsirka, K.; Paipetis, A. S.; Papakonstantinou, P. Radially Grown Graphene Nanoflakes on Carbon Fibers as Reinforcing Interface for Polymer Composites. *ACS Appl. Nano Mater.* **2020**, DOI: 10.1021/acsanm.9b02536.
(29) Shang, N. G.; Papakonstantinou, P.; McMullan, M.; Chu, M.; Stamboulis, A.; Potenza, A.; Dhesi, S. S.; Marchetto, H. Catalyst-Free Efficient Growth, Orientation and Biosensing Properties of Multilayer Graphene Nanoflake Films with Sharp Edge Planes. *Adv. Funct. Mater.* **2008**, *18*, 3506−3514.
(30) Yen, H.-F.; Horng, Y.-Y.; Hu, M.-S.; Yang, W.-H.; Wen, J.-R.; Ganguly, A.; Tai, Y.; Chen, K.-H.; Chen, L.-C. Vertically Aligned Epitaxial Graphene Nanowalls with Dominated Nitrogen Doping for Superior Supercapacitors. *Carbon* **2015**, *82*, 124−134.
(31) Hulicova-Jurcakova, D.; Seredych, M.; Lu, G. Q.; Bandosz, T. J. Combined Effect of Nitrogen- and Oxygen-Containing Functional Groups of Microporous Activated Carbon on Its Electrochemical Performance in Supercapacitors. *Adv. Funct. Mater.* **2009**, *19*, 438−447.
(32) Sun, L.; Wang, L.; Tian, C.; Tan, T.; Xie, Y.; Shi, K.; Li, M.; Fu, H. Nitrogen-Doped Graphene with High Nitrogen Level Via a One-Step Hydrothermal Reaction of Graphene Oxide with Urea for Superior Capacitive Energy Storage. *RSC Adv.* **2012**, *2*, 4498−4506.
(33) Kumar, A.; Ganguly, A.; Papakonstantinou, P. Thermal Stability Study of Nitrogen Functionalities in a Graphene Network. *J. Phys.: Condens. Matter* **2012**, *24*, 235503.
(34) *ASTM D3039/D3039M-17, Standard Test Method for Tensile Properties of Polymer Matrix Composite Materials*; ASTM International: West Conshohocken, PA, 2017.
(35) Bo, Z.; Yang, Y.; Chen, J.; Yu, K.; Yan, J.; Cen, K. Plasma-Enhanced Chemical Vapor Deposition Synthesis of Vertically Oriented Graphene Nanosheets. *Nanoscale* **2013**, *5*, 5180−5204.
(36) Malesevic, A.; Vitchev, R.; Schouteden, K.; Volodin, A.; Zhang, L.; Tendeloo, G. V.; Vanhulsel, A.; Haesendonck, C. V. Synthesis of Few-Layer Graphene Via Microwave Plasma-Enhanced Chemical Vapour Deposition. *Nanotechnology* **2008**, *19*, 305604.
(37) Zhao, J.; Shaygan, M.; Eckert, J.; Meyyappan, M.; Rümmeli, M. H. A Growth Mechanism for Free-Standing Vertical Graphene. *Nano Lett.* **2014**, *14*, 3064−3071.
(38) Thornton, J. D. *Carbon Nanowalls: Processing, Structure and Electrochemical Properties*. Doctor of Philosophy Ph.D. Thesis, North Carolina State University: Raleigh, NC, 2011.
(39) Ni, Z. H.; Fan, H. M.; Feng, Y. P.; Shen, Z. X.; Yang, B. J.; Wu, Y. H. Raman Spectroscopic Investigation of Carbon Nanowalls. *J. Chem. Phys.* **2006**, *124*, 204703.
(40) Ghosh, S.; Ganesan, K.; Polaki, S. R.; Mathews, T.; Dhara, S.; Kamruddin, M.; Tyagi, A. K. Influence of Substrate on Nucleation and Growth of Vertical Graphene Nanosheets. *Appl. Surf. Sci.* **2015**, *349*, 576−581.
(41) Ghosh, S.; Polaki, S. R.; Kumar, N.; Amirthapandian, S.; Kamruddin, M.; Ostrikov, K. Process-Specific Mechanisms of Vertically Oriented Graphene Growth in Plasmas. *Beilstein J. Nanotechnol.* **2017**, *8*, 1658−1670.
(42) Ganguly, A.; Sharma, S.; Papakonstantinou, P.; Hamilton, J. Probing the Thermal Deoxygenation of Graphene Oxide Using High-Resolution in Situ X-Ray-Based Spectroscopies. *J. Phys. Chem. C* **2011**, *115*, 17009−17019.
(43) Hudak, N. S.; Schlichting, A. D.; Eisenbeiser, K. Structural Supercapacitors with Enhanced Performance Using Carbon Nanotubes and Polyaniline. *J. Electrochem. Soc.* **2017**, *164*, A691−A700.
(44) Liu, H.-Y.; Wang, K.-P.; Teng, H. A Simplified Preparation of Mesoporous Carbon and the Examination of the Carbon Accessibility for Electric Double Layer Formation. *Carbon* **2005**, *43*, 559−566.
(45) Akinwolemiwa, B.; Peng, C.; Chen, G. Z. Redox Electrolytes in Supercapacitors. *J. Electrochem. Soc.* **2015**, *162*, A5054−A5059.
(46) Brousse, T.; Bélanger, D.; Long, J. W. To Be or Not to Be Pseudocapacitive? *J. Electrochem. Soc.* **2015**, *162*, A5185−A5189.
(47) Laheäär, A.; Przygocki, P.; Abbas, Q.; Béguin, F. Appropriate Methods for Evaluating the Efficiency and Capacitive Behavior of Different Types of Supercapacitors. *Electrochem. Commun.* **2015**, *60*, 21−25.
(48) Carlson, T.; Asp, L. E. Structural Carbon Fibre Composite/PET Capacitors − Effects of Dielectric Separator Thickness. *Composites, Part B* **2013**, *49*, 16−21.

https://dx.doi.org/10.1021/acsaem.9b02469
ACS Appl. Energy Mater. XXXX, XXX, XXX−XXX